

PROTON AND Λ -HYPERON PRODUCTION IN NUCLEUS-NUCLEUS COLLISIONS

G.H. Arakelyan¹, C. Merino², and Yu.M. Shabelski³

¹A.Alikhanyan National Scientific Laboratory
(Yerevan Physics Institut)
Yerevan, 0036, Armenia
E-mail: argev@mail.yerphi.am

²Departamento de Física de Partículas, Facultade de Física
and Instituto Galego de Física de Altas Enerxías (IGFAE)
Universidade de Santiago de Compostela
15782 Santiago de Compostela
Galiza-Spain
E-mail: merino@fpaxp1.usc.es

³Petersburg Nuclear Physics Institute
NCR Kurchatov Institute
Gatchina, St.Petersburg 188350, Russia
E-mail: shabelsk@thd.pnpi.spb.ru

Abstract

The experimental data on net proton and net Λ -hyperon spectra obtained by the NA35 Collaboration, as well as the inclusive densities of Λ and $\bar{\Lambda}$ obtained by NA49, NA57, and STAR collaborations, are compared with the predictions of the Quark-Gluon String Model. The contributions of String Junction diffusion, interactions with nuclear clusters, and the inelastic screening corrections are accounted for. The level of numerical agreement of the calculations with the experimental data is of about 20–30%. The predictions for LHC are also presented.

PACS. 25.75.Dw Particle and resonance production

1 Introduction

The Quark-Gluon String Model (QGSM) [1] is based on the Dual Topological Unitarization, Regge phenomenology, and nonperturbative notions of QCD. This model is successfully used for the description of multiparticle production processes in hadron-hadron [2, 3, 4, 5], hadron-nucleus [6, 7], and nucleus-nucleus [8, 9, 10] collisions. In particular, the rapidity dependence of inclusive densities of different secondaries (π^\pm , K^\pm , p , and \bar{p}) produced in Pb-Pb collisions at 158 GeV/c per nucleon were reasonably described in ref. [10]. In the present paper we consider the yields of p and \bar{p} , as well as Λ and $\bar{\Lambda}$, produced in the collisions of different nuclei at CERN SpS and RHIC energies.

In the QGSM high energy interactions are considered as proceeding via the exchange of one or several Pomerons, and all elastic and inelastic processes result from cutting through or between Pomerons [11]. Inclusive spectra of hadrons are related to the corresponding fragmentation functions of quarks and diquarks, which are constructed using the Reggeon counting rules [12].

In the case of interaction with nuclear target, the Multiple Scattering Theory (Gribov-Glauber Theory) is used. It allows to consider the interaction with nucleus as the superposition of interactions with different numbers of target nucleons [13, 14, 15, 16].

Also in the case of nucleus-nucleus collisions the Multiple Scattering Theory allows to consider the interaction as the superposition of separate nucleon-nucleon interactions. Though in this case the analytical summation of all the diagrams is impossible [17], the significant classes of diagrams can be analytically summed up in the so-called rigid target approximation [18] which is used in the present paper.

The significant differences in the yields of baryons and antibaryons in the central (midrapidity) region are present even at high energies. This effect can be explained [4, 5, 19, 20, 21, 22, 23, 24] in QGSM by the special structure of baryons consisting of three valence quarks together with a special configuration of gluon field, called String Junction [25, 26, 27, 28].

One additional contribution comes from the coherent interaction of a projectile with multiquark clusters inside the nuclei. The existence of these interactions is confirmed by the presence, with not such a small probability, of a cumulative effect [29].

These contributions were incorporated into the QGSM in [30, 31], and they allow to describe a number of experimental facts.

At very high energies the contribution of the enhancement Reggeon diagrams be-

comes important, leading to a new phenomenological effect, the suppression of the inclusive density of secondaries [32] in the central (midrapidity) region.

In this paper we present the description of p , \bar{p} , Λ , and $\bar{\Lambda}$ production on nuclear targets at CERN SpS and RHIC energies.

2 Baryon/antibaryon asymmetry in the QGSM

2.1 General approach

The QGSM [1, 2, 3] allows one to make quantitative predictions for different features of multiparticle production, in particular, for the inclusive densities of different secondaries, both in the central and in the beam fragmentation regions.

In QGSM, each exchanged Pomeron corresponds to a cylindrical diagram, and thus, when cutting one Pomeron, two showers of secondaries are produced (see Fig. 1 a,b).

The inclusive spectrum of a secondary hadron h is then determined by the convolution of the diquark, valence quark, and sea quark distributions, $u(x, n)$, in the incident particles, with the fragmentation functions, $G^h(z)$, of quarks and diquarks into the secondary hadron h . Both the distributions and the fragmentation functions are constructed using the Reggeon counting rules.

In particular, in the case of $n > 1$, i.e. in the case of multipomeron exchange, the distributions of valence quarks and diquarks are softened due to the appearance of a sea quark contribution. There is some freedom [6] in how to account for this effect. In principle, the valence and sea quarks can depend on n in a different manner, for example:

$$\begin{aligned}
 u_{uu}(x, n) &= C_{uu} \cdot x^{\alpha_R - 2\alpha_B + 1} \cdot (1 - x)^{-\alpha_R + m_1} \\
 u_{ud}(x, n) &= C_{ud} \cdot x^{\alpha_R - 2\alpha_B} \cdot (1 - x)^{-\alpha_R + m_2} \\
 u_u(x, n) &= C_u \cdot x^{-\alpha_R} \cdot (1 - x)^{\alpha_R - 2\alpha_B + m_2} \\
 u_d(x, n) &= C_d \cdot x^{-\alpha_R} \cdot (1 - x)^{\alpha_R - 2\alpha_B + 1 + m_1} \\
 u_s(x, n) &= C_d \cdot x^{-\alpha_R} \cdot (1 - x)^{\alpha_R - 2\alpha_B + (n-1) + d}, \tag{1}
 \end{aligned}$$

where every distribution $u_i(x, n)$ is normalized to unity, d is a parameter, and the values of m_1 and m_2 can be found from the conditions:

$$\langle x_{uu} \rangle + \langle x_d \rangle + 2(n - 1) \cdot \langle x_s \rangle = 1$$

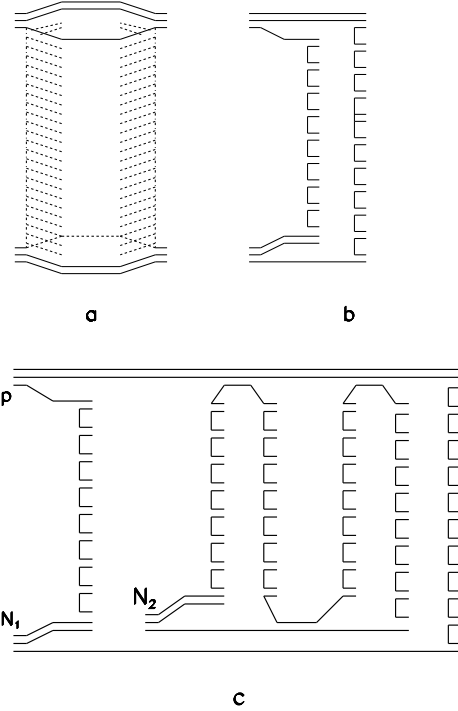


Figure 1: (a) Cylindrical diagram representing a Pomeron exchange within the DTU classification (quarks are shown by solid lines); (b) One cut of the cylindrical diagram corresponding to the single-Pomeron exchange contribution in inelastic pp scattering; (c) One of the diagrams for the inelastic interaction of one incident proton with two target nucleons N_1 and N_2 in a pA collision.

$$\langle x_{ud} \rangle + \langle x_u \rangle + 2(n-1) \cdot \langle x_s \rangle = 1. \quad (2)$$

The details of the model are presented in [1, 2, 3, 19]. The averaged number of exchanged Pomerons $\langle n \rangle_{pp}$ slowly increase with the energy. The Pomeron parameters have been taken from [3].

For a nucleon target, the inclusive rapidity, y , or Feynman- x , x_F , spectrum of a secondary hadron h has the form [1]:

$$\frac{dn}{dy} = \frac{x_E}{\sigma_{inel}} \cdot \frac{d\sigma}{dx_F} = \sum_{n=1}^{\infty} w_n \cdot \phi_n^h(x) + w_D \cdot \phi_D^h(x), \quad (3)$$

where the functions $\phi_n^h(x)$ determine the contribution of diagrams with n cut Pomerons, w_n is the relative weight of this diagram, and the term $w_D \cdot \phi_D^h(x)$ accounts for the contribution of diffraction dissociation processes.

In the case of pp collisions:

$$\phi_n^h(x) = f_{qq}^h(x_+, n) \cdot f_q^h(x_-, n) + f_q^h(x_+, n) \cdot f_{qq}^h(x_-, n) + 2(n-1) \cdot f_s^h(x_+, n) \cdot f_s^h(x_-, n) , \quad (4)$$

$$x_{\pm} = \frac{1}{2}[\sqrt{4m_T^2/s + x^2} \pm x] , \quad (5)$$

where f_{qq} , f_q , and f_s correspond to the contributions of diquarks, valence quarks, and sea quarks, respectively.

These contributions are determined by the convolution of the diquark and quark distributions with the fragmentation functions, e.g.,

$$f_q^h(x_+, n) = \int_{x_+}^1 u_q(x_1, n) \cdot G_q^h(x_+/x_1) dx_1 . \quad (6)$$

In the calculation of the inclusive spectra of secondaries produced in pA collisions we should consider the possibility of one or several Pomeron cuts in each of the ν blobs of proton-nucleon inelastic interactions. For example, in Fig. 1c it is shown one of the diagrams contributing to the inelastic interaction of a beam proton with two target nucleons. In the blob of the proton-nucleon1 interaction one Pomeron is cut, while in the blob of the proton-nucleon2 interaction two Pomerons are cut. The contribution of the diagram in Fig. 1c to the inclusive spectrum is

$$\begin{aligned} \frac{x_E}{\sigma_{prod}^{pA}} \cdot \frac{d\sigma}{dx_F} &= 2 \cdot W_{pA}(2) \cdot w_1^{pN_1} \cdot w_2^{pN_2} \cdot \{ f_{qq}^h(x_+, 3) \cdot f_q^h(x_-, 1) + \\ &+ f_q^h(x_+, 3) \cdot f_{qq}^h(x_-, 1) + f_s^h(x_+, 3) \cdot [f_{qq}^h(x_-, 2) + f_q^h(x_-, 2) + \\ &+ 2 \cdot f_s^h(x_-, 2)] \} , \end{aligned} \quad (7)$$

where $W_{pA}(2)$ is the probability of interaction with namely two target nucleons.

It is essential to take into account all digrams with every possible Pomeron configuration and its corresponding permutations. The diquark and quark distributions and the fragmentation functions are the same as in the case of pN interaction.

The total number of exchanged Pomerons becomes as large as

$$\langle n \rangle_{pA} \sim \langle \nu \rangle_{pA} \cdot \langle n \rangle_{pN} , \quad (8)$$

where $\langle \nu \rangle_{pA}$ is the average number of inelastic collisions inside the nucleus (about 4 for heavy nuclei at SpS energies).

The process shown in Fig. 1c satisfies [13, 14, 15, 16] the condition that the absorptive parts of the hadron-nucleus amplitude are determined by the combination of the absorptive parts of the hadron-nucleon amplitudes.

In the case of a nucleus-nucleus collision, in the fragmentation region of projectile we use the approach [8, 9, 10], where the beam of independent nucleons of the projectile interact with the target nucleus, what corresponds to the rigid target approximation [18] of Glauber Theory. In the target fragmentation region, on the contrary, the beam of independent target nucleons interact with the projectile nucleus, these two results coinciding in the central region. The corrections for energy conservation play here a very important role if the initial energy is not very high. This approach was used in [10] for the successful description of π^\pm , K^\pm , p , and \bar{p} produced in Pb-Pb collisions at 158 GeV per nucleon.

In the present paper we consider the spectra of secondary baryons and antibaryons, as well as their differences, i.e. the net baryon spectra. At low energies, the net baryon spectra coincide with the spectra of baryon, while at asymptotically high energies they are negligible due to the even signature of the Pomeron trajectory. The energy dependence of the net baryon spectra between these two limits strongly depends on the production mechanism.

2.2 String Junction contribution

In the string models, baryons are considered as configurations consisting of three connected strings (related to three valence quarks), called String Junction (SJ) [25, 26, 27, 28], this picture leading to some quite general phenomenological predictions.

The production of a baryon-antibaryon pair in the central region usually occurs via $SJ\text{-}\overline{SJ}$ pair production (SJ has upper color indices, whereas anti-SJ (\overline{SJ}) has lower indices), which then combines with sea quarks and sea antiquarks into a $B\bar{B}$ pair [27, 33], as it is shown in Fig. 2a.

However, in the processes with incident baryons there exists another possibility to produce a secondary baryon in the central region, called SJ diffusion. The quantitative description of the baryon number transfer due to SJ diffusion in rapidity space was obtained in [19] and following papers [4, 5, 20, 21, 22, 24].

In the QGSM the differences in the spectra of secondary baryons and antibaryons appear for processes which present SJ diffusion in rapidity space. These differences only vanish rather slowly when the energy increases.

To obtain the net baryon charge, and according to ref. [19], we consider three

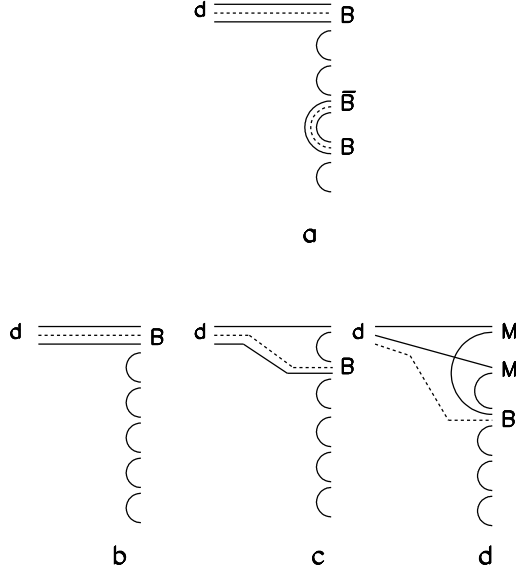


Figure 2: QGSM diagrams describing secondary baryon production: (a) usual $B\bar{B}$ central production with production of new SJ pair; (b) initial SJ together with two valence quarks and one sea quark; (c) initial SJ together with one valence quark and two sea quarks; (d) initial SJ together with three sea quarks.

different possibilities. The first one is the fragmentation of the diquark giving rise to a leading baryon (Fig. 2b). A second possibility is to produce a leading meson in the first break-up of the string and a baryon in a subsequent break-up [12, 34] (Fig. 2c). In these two first cases the baryon number transfer is possible only for short distances in rapidity. In the third case, shown in Fig. 2d, both initial valence quarks recombine with sea antiquarks into mesons, M , while a secondary baryon is formed by the SJ together with three sea quarks [5, 19, 35].

The fragmentation functions for the secondary baryon B production corresponding to the three processes shown in Fig. 2b, 2c, and 2d can be written as follows (see [19] for more details):

$$G_{qq}^B(z) = a_N \cdot v_{qq}^B \cdot z^{2.5}, \quad (9)$$

$$G_{qs}^B(z) = a_N \cdot v_{qs}^B \cdot z^2 \cdot (1-z), \quad (10)$$

$$G_{ss}^B(z) = a_N \cdot \varepsilon \cdot v_{ss}^B \cdot z^{1-\alpha_{SJ}} \cdot (1-z)^2, \quad (11)$$

where a_N is the normalization parameter, and v_{qq}^B , v_{qs}^B , v_{ss}^B are the relative probabilities for different baryons production that can be found by simple quark combinatorics [36, 37]. These probabilities depend on the strangeness suppression factor S/L , and we use $S/L = 0.32$ following [38].

The contribution of the graph in Fig. 2d has in QGSM a coefficient ε which determines the small probability for such a baryon number transfer.

The fraction z of the incident baryon energy carried by the secondary baryon decreases from Fig. 2b to Fig. 2d. Only the processes in Fig. 2d can contribute to the inclusive spectra in the central region at high energies if the value of the intercept of the SJ exchange Regge-trajectory, α_{SJ} , is large enough. The analysis in [24] gives a value of $\alpha_{SJ} = 0.5 \pm 0.1$, that is in agreement with the ALICE Collaboration result, $\alpha_{SJ} \sim 0.5$ [39], obtained at LHC. In the calculations of these effects we use the following values of the parameters [24]:

$$\alpha_{SJ} = 0.5 \quad \text{and} \quad \varepsilon = 0.0757. \quad (12)$$

2.3 Contribution from interaction with clusters

In the case of interaction with a nuclear target some secondaries can be produced in the kinematical region forbidden for the interaction with a free nucleon. Such processes are called the cumulative ones, the simplest example being the production of secondary nucleons in the backward hemisphere in the laboratory frame.

Usually, the cumulative processes are considered as a result of the coherent interaction of a projectile with a multiquark cluster, i.e. with a group of several nucleons which are at short distances from each other that appears as a fluctuation of the nuclear matter [29, 40].

The inclusive spectra of the secondary hadron h in the central region is determined at high energies by double-Pomeron diagrams [41]. The case of pp collision is shown in Fig. 3a. In the case of proton-nucleus collisions two different possibilities exist, the interactions with individual target nucleons (Fig. 3b) and the secondary production on cluster (Fig. 3c). For nucleus-nucleus collisions there are four possibilities (Figs. 3d, 3e, 3f, and 3g). The one in Fig. 3g corresponds to a new process where a secondary hadron is produced by the interaction of two clusters.

It was shown in refs. [30, 31] that in the case of secondary production from the cluster fragmentation, the inclusive spectra can be calculated in the framework of the QGSM with the same quark and diquark fragmentation functions. The only difference comes from the quark and diquark distributions, $u_q^{cl}(x, n, k)$ and $u_{qq}^{cl}(x, n, k)$, where k is the number of nucleons in the cluster. The distributions $u_i^{cl}(x, n, k)$ can also be calculated by using the Reggeon counting rules, and they take the form:

$$\begin{aligned} u_{uu}^{cl}(x, n) &= C_{uu} \cdot x^{\alpha_R - 2\alpha_B + 1} \cdot (k - x)^{-\alpha_R N + m_1} \\ u_{ud}^{cl}(x, n) &= C_{ud} \cdot x^{\alpha_R - 2\alpha_B} \cdot (k - x)^{-\alpha_R + N + m_2} \end{aligned}$$

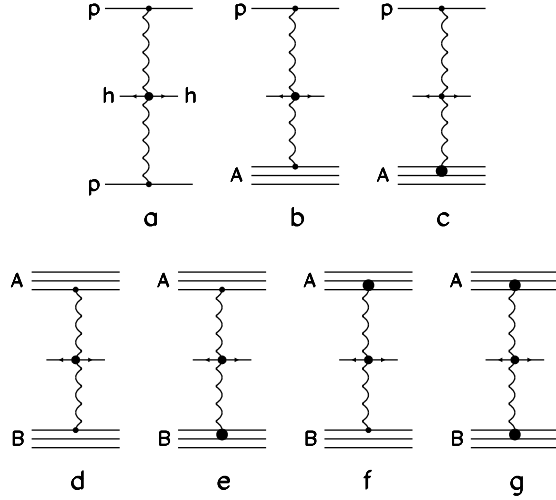


Figure 3: Reggeon diagrams for the different possibilities corresponding to the inclusive spectra of a secondary hadron h produced in the central region in (a) pp , (b,c) pA , and (d–g) AB collisions. Pomerons are shown by wavy lines.

$$\begin{aligned}
u_u^{cl}(x, n, k) &= C_u \cdot x^{-\alpha_R} \cdot (k - x)^{\alpha_R - 2\alpha_B + N + m_2} \\
u_d^{cl}(x, n) &= C_d \cdot x^{-\alpha_R} \cdot (k - x)^{\alpha_R - 2\alpha_B + 1 + N + m_1} \\
u_s^{cl}(x, n) &= C_d \cdot x^{-\alpha_R} \cdot (1 - x)^{\alpha_R - 2\alpha_B + (n-1) + d} ,
\end{aligned} \tag{13}$$

where

$$N = 2 \cdot (1 - \alpha_B) \cdot (k - 1) . \tag{14}$$

The function $u_s^{cl}(x, n)$ does not depend on k . All these functions $u_i^{cl}(x, n, k)$ are normalized to unity and the values m_1 and m_2 can be found from conditions in Eq. (2).

This approach was successfully used in [30, 31] for the description of cumulative particles produced in hA collisions. In the present paper we use it for describing the enhancement of strangeness production on nuclear targets in the central region.

The probability to find a proton in the backward hemisphere in high energy pA collisions reach values up to 10%. Keeping in mind that it is only a part of cumulative processes, in the numerical calculations and for every hadron-nucleon interaction we take the probability to interact with a cluster V^{cl} , and the probability to actually interact with a nucleon $1 - V^{cl}$. We use the numerical values:

$$V^{cl} = 0.2 \text{ (for mediumA) } , V^{cl} = 0.3 \text{ (for heavyA) } , \tag{15}$$

as the maximal reasonable values of V^{cl} .

2.4 Inelastic screening (percolation) effects

The QGSM gives a reasonable description [5, 6, 10, 42] of the inclusive spectra of different secondaries produced both in hadron-nucleus and in nucleus-nucleus collisions at energies $\sqrt{s_{NN}} = 14\text{--}30$ GeV.

At RHIC energies the situation drastically changes. The spectra of secondaries produced in pp collisions are described rather well [5], but the RHIC experimental data for Au+Au collisions [43, 44] give clear evidence of the inclusive density suppression effects which reduce by a factor ~ 0.5 the midrapidity inclusive density, when compared to the predictions based on the superposition picture [45, 46, 47]. This reduction can be explained by the inelastic screening corrections connected to multipomeron interactions [32] (see Fig. 4).

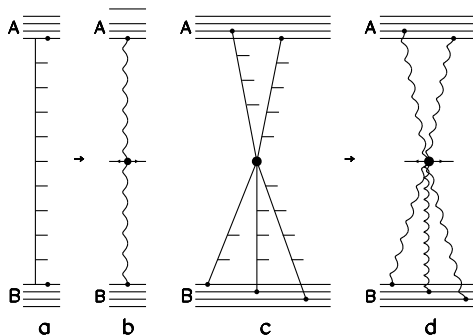


Figure 4: (a) Multiperipheral ladder corresponding to the inclusive cross section of diagram (b), and (c) fusion of several ladders corresponding to the inclusive cross section of diagram (d).

At energies $\sqrt{s_{NN}} \leq 30\text{--}40$ GeV, the inelastic processes are determined by the production of one (Fig. 4a) or several (Fig. 4c) multiperipheral ladders, and the corresponding inclusive cross sections are described by the diagrams of Fig. 4b and Fig. 4d.

In accordance with the Parton Model [48, 49], the fusion of multiperipheral ladders shown in Fig. 4c becomes more and more important with the increase of the energy, resulting in the reduction of the inclusive density of secondaries. Such processes correspond to the enhancement Reggeon diagrams of the type of Fig. 4d, and to even more complicate ones. All these diagrams are proportional to the squared longitudinal form factors of both colliding nuclei [32], so their contribution becomes negligible when the energy decreases. Following the estimations presented in reference [32], the RHIC energies are just of the order of magnitude needed to observe this effect.

However, all quantitative estimations are model dependent. The numerical weight

of the contribution of the multipomeron diagrams is rather unclear due to the many unknown vertices in these diagrams. The number of unknown parameters can be reduced in some models, and, as an example, in reference [32] the Schwimmer model [50] was used for the numerical estimations. Also, in [51] the phenomenological multipomeron vertices of eikonal type were introduced for the summation of the enhancement diagram.

Another possibility to estimate the contribution of the diagrams with Pomeron interaction comes [52, 53, 54, 55, 56] from Percolation Theory. The percolation approach and its previous version, the String Fusion Model [57, 58, 59], predicted the multiplicity suppression seen at RHIC energies, long before any RHIC data were measured.

New calculations of inclusive densities and multiplicities in percolation theory both in pp [60, 61], and in heavy ion collisions [61, 62], are in good agreement with the experimental data in a wide energy region.

In order to account for the percolation (inelastic screening) effects in the QGSM, it is technically more simple [23] to consider the maximal number of Pomerons n_{max} emitted by one nucleon in the central region that can be cut. These cut Pomerons lead to the different final states. Then the contributions of all diagrams with $n \leq n_{max}$ are accounted for as at lower energies. The larger number of Pomerons $n > n_{max}$ can also be emitted obeying the unitarity constraint, but due to the fusion in the final state (at the quark-gluon string stage), the cut of $n > n_{max}$ Pomerons results in the same final state as the cut of n_{max} Pomerons.

By doing this, all model calculations become very similar to the percolation approach. The QGSM fragmentation formalism allows one to calculate the integrated over p_T spectra of different secondaries as the functions of rapidity and x_F .

In this frame, we obtain a reasonable agreement with the experimental data on the inclusive spectra of secondaries produced in d+Au collisions at RHIC energy [23] with a value $n_{max} = 13$, and in p+Pb collisions at LHC energy [63] with the value $n_{max} = 23$. It has been shown in [64] that the number of strings that can be used for the secondary production should increase with the initial energy.

3 Numerical results

3.1 Net baryon spectra

One example of the QGSM description of the x_F -spectra of secondary protons and antiprotons measured in pp collisions at 158 GeV/c by NA49 Collaboration [65] is presented in Fig. 5.

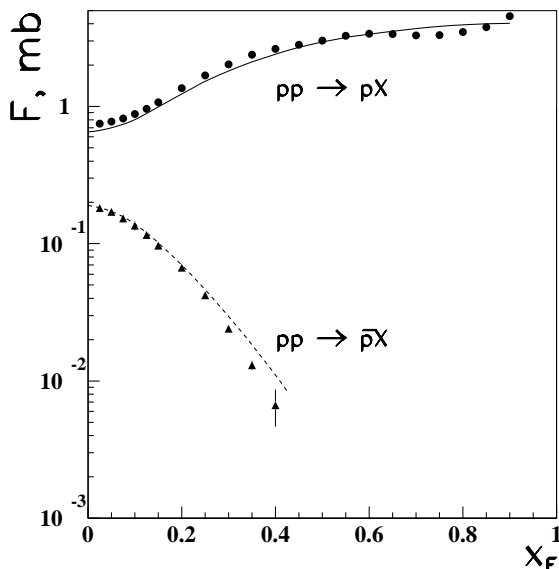


Figure 5: QGSM x_F -spectra of secondary protons and antiprotons produced in pp collisions at 158 GeV/c compared to the experimental data by the NA49 Collaboration [65].

The QGSM results for net proton ($p - \bar{p}$) and net Λ -hyperon ($\Lambda - \bar{\Lambda}$) productions at 200 GeV per nucleon are compared to the experimental data by the NA35 Collaboration [66] in Figs. 6 and 7.

The data for net baryon production by proton beam interaction with ^{32}S and ^{197}Au nuclear targets are presented in Fig. 6 in the central and beam fragmentation regions as function of rapidity in the laboratory system. The absolute normalization of dn/dy in all cases is determined by the data of proton and antiproton production in pp collisions at similar energies.

The results of the QGSM calculations without SJ and cluster contributions are

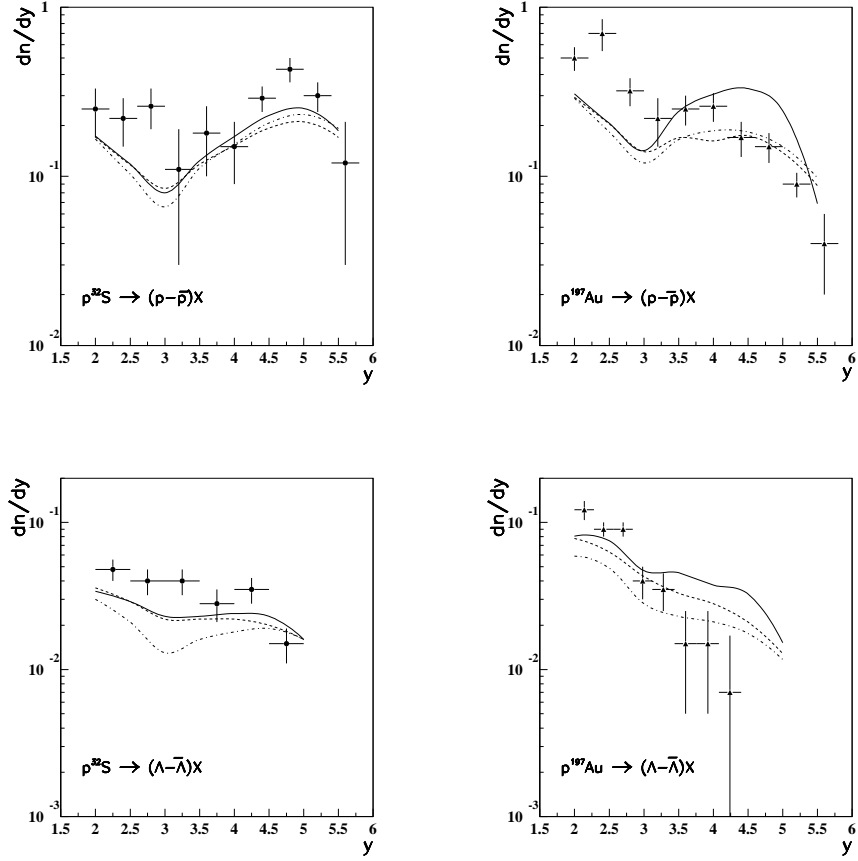


Figure 6: Net proton $p - \bar{p}$ (upper panels) and net Λ -hyperon $\Lambda - \bar{\Lambda}$ (lower panels) production in $p-^{32}\text{S}$ (left panels) and $p-^{197}\text{Au}$ (right panels) collisions at 200 GeV per nucleon. Solid curves show the QGSM calculations with both SJ and cluster contributions, dashed curves with SJ contributions but without the cluster ones, and dotted curves without both SJ and cluster contributions.

shown in Fig. 6 by dotted lines. Dashed lines show the same calculations with SJ contributions but without the cluster ones, and solid lines show the results with both SJ and cluster contributions. The corrections for very high energy interactions described in Subsection 2.4 are negligible at this energy.

In the case of net proton production in $p-^{32}\text{S}$ collisions, all three curves are close to each other and they are in reasonable agreement with the experimental data. In the case of $p-^{197}\text{Au}$ collisions the number of net protons is too small at small rapidities, what can be explained by the influence of the target fragmentation region. The nuclear cluster contribution, which is important mainly in the beam fragmentation region, seems to be too large.

In the case of net Λ -hyperon production the experimental error bars are rather large,

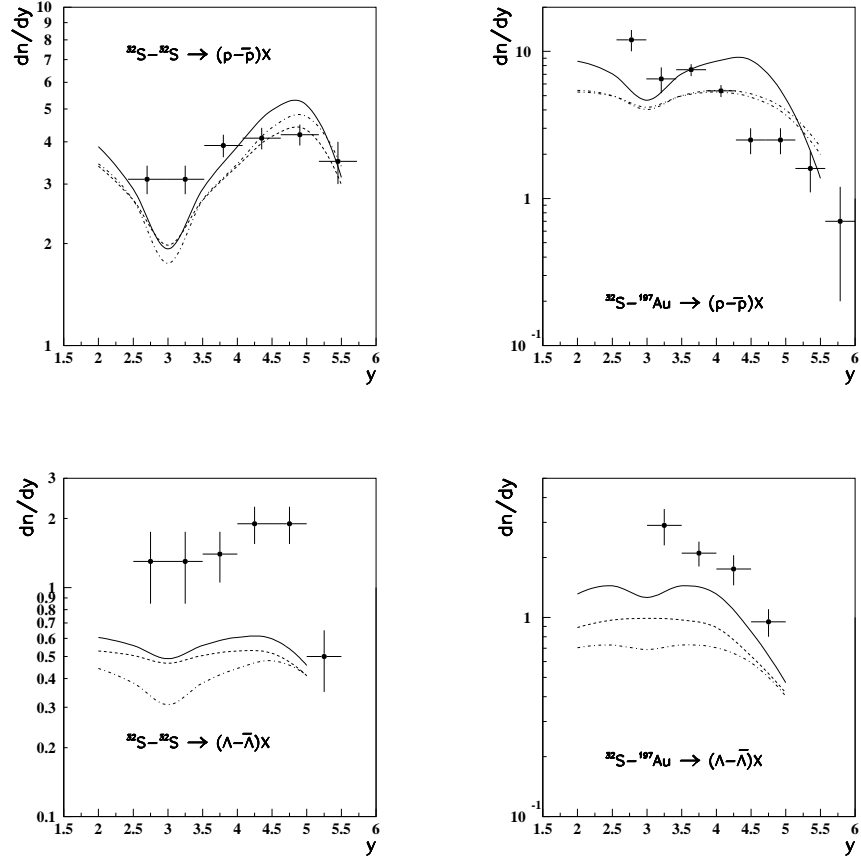


Figure 7: Net proton $p-\bar{p}$ (upper panels) and net Λ -hyperon $\Lambda-\bar{\Lambda}$ (lower panels) production in $^{32}\text{S}-^{32}\text{S}$ (left panels) and in $^{32}\text{S}-^{197}\text{Au}$ (right panels) collisions at 200 GeV per nucleon. Solid curves show the QGSM calculations with both SJ and cluster contributions, dashed curves with SJ contributions but without the cluster ones, and dotted curves without both SJ and cluster contributions.

and one can talk of general semiquantitative agreement of the QGSM calculations with the data in the lower panels of Fig. 6.

For the sulphur ^{32}S beam shown in Fig. 7, the theoretical calculations are in reasonable agreement with the data for net proton production, whereas the data on net Λ -hyperon production are systematically higher than all calculated curves. In any case, though, all disagreements are not large than $\sim 30\%$.

The data of the NA35 Collaboration [66] are compatible with the results of the NA44 Collaboration [67].

3.2 Λ and $\bar{\Lambda}$ production in midrapidity region

The NA49 Collaboration obtained experimental data [68] for yields of Λ and $\bar{\Lambda}$ hyperons in midrapidity region ($|y| < 0.4$) in the central C+C, Si+Si, and Pb+Pb collisions (5% centrality), at 158 GeV per nucleon. These results are presented in Table 1, together with the QGSM results obtained for the same rapidities and centralities.

\sqrt{s} (GeV)	Reaction	QGSM	Experiment dn/dy
17.2	C + C \rightarrow Λ	0.237	$0.24 \pm 0.01 \pm 0.04$, [68]
	C + C \rightarrow $\bar{\Lambda}$	0.064	$0.064 \pm 0.003 \pm 0.010$ [68]
17.2	Si + Si \rightarrow Λ	0.69	$0.68 \pm 0.04 \pm 0.13$, [68]
	Si + Si \rightarrow $\bar{\Lambda}$	0.17	$0.16 \pm 0.007 \pm 0.038$, [68]
17.2	Pb + Pb \rightarrow Λ	9.4	$12.9 \pm 0.7 \pm 1.5$ [68]
	Pb + Pb \rightarrow $\bar{\Lambda}$	2.05	$1.4 \pm 0.3 \pm 0.2$ [68]
17.2 (m.b.)	p + Be \rightarrow Λ	0.034	$0.034 \pm 0.0005 \pm 0.003$ [69]
	p + Be \rightarrow $\bar{\Lambda}$	0.010	$0.011 \pm 0.0002 \pm 0.001$ [69]
17.2 (m.b.)	p + Pb \rightarrow Λ	0.074	$0.060 \pm 0.002 \pm 0.006$ [69]
	p + Pb \rightarrow $\bar{\Lambda}$	0.0019	$0.015 \pm 0.001 \pm 0.002$ [69]
17.2	Pb + Pb \rightarrow Λ	9.4	$18.5 \pm 1.1 \pm 1.8$ [69]
	Pb + Pb \rightarrow $\bar{\Lambda}$	2.05	$2.44 \pm 0.14 \pm 0.24$ [69]
62.4	Au + Au \rightarrow Λ	11.1	$15.7 \pm 0.3 \pm 2.3$ [70]
	Au + Au \rightarrow $\bar{\Lambda}$	8.2	$8.3 \pm 0.2 \pm 1.1$ [70]
200	Cu + Cu \rightarrow Λ	3.82	4.68 ± 0.45 [71]
	Cu + Cu \rightarrow $\bar{\Lambda}$	3.34	3.79 ± 0.37 [71]
200	Au + Au \rightarrow Λ	14.2	14.8 ± 2.4 [71]
	Au + Au \rightarrow $\bar{\Lambda}$	12.1	11.7 ± 0.9 [71]
3000	Pb + Pb \rightarrow Λ	36.2	-
	Pb+Pb \rightarrow $\bar{\Lambda}$	35.6	-

Table 1. Experimental NA49 [68], NA57 [69], and STAR [70, 71] data for Λ and $\bar{\Lambda}$ production at 158GeV per nucleon, and at STAR energies, and the corresponding description by the QGSM.

On the other hand, the NA57 Collaboration obtained the experimental data [69] for Λ and $\bar{\Lambda}$ yields in midrapidity region $|y| < 0.5$ in the minimum bias p +Be and p +Pb interactions, and in central (5% centrality) Pb+Pb collisions at 158 GeV per nucleon.

Unfortunately, the data by the NA49 and NA57 Collaborations are not compatible, as one can see from Table 1, where the values of dn/dy for different hyperons measured

by one collaboration are far outside the error bars of the corresponding values published by the other collaboration for the same centrality. This is probably due to different experimental event selection. .

Here again one can see that the calculated yields of Λ and $\bar{\Lambda}$ are in agreement with experimental data on the level of 20–30% accuracy.

Hyperon production at higher energies in midrapidity region was also measured at RHIC. The data by the STAR Collaboration [70, 71] for Au + Au and Cu+Cu collisions at $\sqrt{s_{NN}} = 62.4$ GeV and 200 GeV are presented in Table 1. We also give in Table 1 the QGSM predictions for central Pb+Pb collisions at the LHC energy $\sqrt{s_{NN}} = 3$ TeV.

4 Conclusion

The QGSM provides a reasonable description of nucleon and Λ , as well as their antiparticles, production in nucleon-nucleus and nucleus-nucleus collisions at high energies. The level of numerical accuracy is of about 20–30%. Part of the uncertainty is connected to discrepancies among the different experimental data.

Inclusive densities of $\bar{\Xi}^+$ hyperons are reasonably reproduced for the cases of p+Be and p+Pb collisions [69], but they are several times underestimated in the case of central Pb+Pb interactions [69]. For $\bar{\Omega}^+$ production in central Pb+Pb collisions the disagreement is larger than one order of magnitude. The physical reasons for these observed disagreements will be discussed in a separate paper.

Acknowledgements

We are grateful to [A.B. Kaidalov](#) for useful discussions and comments. This paper was supported by Ministerio de Educación y Ciencia of Spain under the Spanish Consolider-Ingenio 2010 Programme CPAN (CSD2007-00042) and project FPA 2005–01963, by Xunta de Galicia and, in part, by grant RSGSS-3628.2008.2, and by the State Committee of Science of the Republic of Armenia, through Grant-11-1C015.

References

- [1] A.B. Kaidalov and K.A. Ter-Martirosyan, *Yad. Fiz.* **39**, 1545 (1984); **40**, 211 (1984).
- [2] A.B. Kaidalov and O.I. Piskounova, *Yad. Fiz.* **41**, 1278 (1985); *Z. Phys.* **C30**, 145 (1986).
- [3] Yu.M. Shabelski, *Yad. Fiz.* **44**, 186 (1986).
- [4] G.H. Arakelyan, C. Merino, C. Pajares, and Yu.M. Shabelski, *Eur. Phys. J.* **C54**, 577 (2008) and hep-ph/0709.3174.
- [5] C. Merino, C. Pajares, and Yu.M. Shabelski, *Eur. Phys. J.* **C71**, 1652 (2011).
- [6] A.B. Kaidalov, K.A. Ter-Martirosyan, and Yu.M. Shabelski, *Yad. Fiz.* **43**, 1282 (1986).
- [7] Yu.M. Shabelski, *Z. Phys.* **C38**, 569 (1988).
- [8] Yu.M. Shabelski, *Yad. Fiz.* **50**, 239 (1989).
- [9] Yu.M. Shabelski, *Z. Phys.* **C57**, 409 (1993).
- [10] J. Dias de Deus and Yu.M. Shabelski, *Yad. Fiz.* **71**, 191 (2008).
- [11] V.A. Abramovsky, V.N. Gribov, and O.V. Kancheli, *Yad. Fiz.* **18**, 595 (1973).
- [12] A.B. Kaidalov, *Sov. J. Nucl. Phys.* **45**, 902 (1987); *Yad. Fiz.* **43**, 1282 (1986).
- [13] Yu.M. Shabelski, *Yad. Fiz.* **26**, 1084 (1977); *Nucl. Phys.* **B132**, 491 (1978).
- [14] L. Bertocchi and D. Treleani, *J. Phys.* **G3**, 147 (1977).
- [15] J. Weis, *Acta Phys. Polonica* **B7**, 85 (1977).
- [16] T. Jaroszewicz *et al.*, *Z. Phys.* **C1**, 181 (1979).
- [17] V.M. Braun and Yu.M. Shabelski, *Int. J. Mod. Phys.* **A3**, 2117 (1988).
- [18] G.D. Alkhazov *et al.*, *Nucl. Phys.* **A280**, 365 (1977).
- [19] G.H. Arakelyan, A. Capella, A.B. Kaidalov, and Yu.M. Shabelski, *Eur. Phys. J.* **C26**, 81 (2002) and hep-ph/0103337.

- [20] F. Bopp and Yu.M. Shabelski, *Yad. Fiz.* **68**, 2155 (2005) and hep-ph/0406158; *Eur. Phys. J. A***28**, 237 (2006) and hep-ph/0603193.
- [21] G.H. Arakelyan, C. Merino, and Yu.M. Shabelski, *Yad. Fiz.* **69**, 911 (2006) and hep-ph/0505100; *Phys. Atom. Nucl.* **70**, 1110 (2007) and hep-ph/0604103; *Eur. Phys. J. A***31**, 519 (2007) and hep-ph/0610264.
- [22] O.I. Piskounova, *Phys. Atom. Nucl.* **70**, 1110 (2007) and hep-ph/0604157.
- [23] C. Merino, C. Pajares, and Yu.M. Shabelski, *Eur. Phys. J. C***59**, 691 (2009). and arXiv:0802.2195 [hep-ph].
- [24] C. Merino, M.M. Ryzhinski, and Yu.M. Shabelski, *Eur. Phys. J. C***62**, 491 (2009); Lecture given by Yu.M. Shabelski at The XLIII PNPI Winter School on Physics, St.Petersburg (Russia), February 2009, arXiv:0906.2659[hep-ph].
- [25] X. Artru, *Nucl. Phys. B***85**, 442 (1975).
- [26] M. Imachi, S. Otsuki, and F. Toyoda, *Prog. Theor. Phys.* **52**, 346 (1974); **54**, 280 (1976); **55**, 551 (1976).
- [27] G.C. Rossi and G. Veneziano, *Nucl. Phys. B***123**, 507 (1977).
- [28] D. Kharzeev, *Phys. Lett. B***378**, 238 (1996).
- [29] L.L. Frankfurt and M.I. Strikman, *Phys. Rep.* **76**, 215 (1981).
- [30] A.V. Efremov *et al.*, *Sov. J. Nucl. Phys.* **47**, 858 (1988).
- [31] A.V. Efremov *et al.*, *Phys. Atom. Nucl.* **57**, 874 (1994).
- [32] A. Capella, A. Kaidalov, and J. Tran Thanh Van, *Heavy Ion Phys.* **9**, 169 (1999).
- [33] S.E. Vance, M. Gyulassy, and X-N. Wang, *Phys. Lett. B***443**, 45 (1998).
- [34] A. Capella and B.Z. Kopeliovich, *Phys. Lett. B***381** 325 (1996).
- [35] B.Z. Kopeliovich and B. Povh, *Z. Phys. C***75**, 693 (1997); *Phys. Lett. B***446**, 321 (1999). *Phys. Lett. B***469**, 9 (2000).
- [36] V.V. Anisovich and V.M. Shekhter, *Nucl. Phys. B***55**, 455 (1973).
- [37] A. Capella and C.A. Salgado, *Phys. Rev. C***60**, 054906 (1999).

- [38] G.H. Arakelyan, A.B. Kaidalov, C. Merino, and Yu.M. Shabelski, Phys. Atom. Nucl. **74**, 126 (2011) and arXiv:1004.4074[hep-ph].
- [39] K. Aamodt *et al.*, ALICE Collaboration, Phys. Rev. Lett. **6015**, 072002 (2010) and arXiv:1006.5432[hep-ex].
- [40] D.I. Blokhintsev, JETP **13**, 1295 (1957).
- [41] V.A. Abramovsky, O.V. Kancheli, and I.D. Mandzhavidze, Sov. J. Nucl. Phys. **13**, 630 (1971); Yad. Fiz. **13**, 1102 (1971).
- [42] Yu.M. Shabelski, Sov. J. Nucl. Phys. **45**, 143 (1987); Z. Phys. C**38**, 569 (1988).
- [43] B.B. Back *et al.*, PHOBOS Collaboration, Phys. Rev. Lett. **85**, 3100 (2000).
- [44] K. Adcox *et al.*, PHENIX Collaboration, Phys. Rev. Lett. **86**, 500 (2001).
- [45] A. Capella, C. Merino, and J. Tran Thanh Van, Phys. Lett. B**265** (1991) 415.
- [46] Yu.M. Shabelski, Z. Phys. C**57**, 409 (1993).
- [47] N. Armesto and C. Pajares, Int. J. Mod. Phys. A**15**, 2019 (2000).
- [48] O.V. Kancheli, JETP Lett. **18**, 274 (1973).
- [49] G.V. Davidenko and N.N. Nikolaev, Yad. Fiz. **24**, 772 (1976).
- [50] A. Schwimmer, Nucl. Phys. B**94**, 445 (1975).
- [51] S. Ostapchenko, Phys. Rev. D**77**, 034009 (2008).
- [52] J. Dias de Deus, R. Ugoccioni, and A. Rodrigues, Phys. Lett. B**458**, 402 (1999).
- [53] J. Dias de Deus, R. Ugoccioni, and A. Rodrigues, Eur. Phys. J. C**16**, 537 (2000).
- [54] M.A. Braun and C. Pajares, Phys. Rev. Lett. **85**, 4864 (2000).
- [55] J. Dias de Deus and Yu.M. Shabelski, Eur. Phys. J. A**20**, 457 (2004).
- [56] P. Brogueira, J. Dias de Deus, and C. Pajares, Phys. Rev. C**75**, 054908 (2007).
- [57] C. Merino, C. Pajares, and J. Ranft, Phys. Lett. B**276**, 168 (1992).
- [58] H.J. Möhring, J. Ranft, C. Merino, and C. Pajares, Phys. Rev. D**47**, 4142 (1993).
- [59] N.S. Amelin, M.A. Braun, and C. Pajares, Z. Phys. C**63**, 507 (1994).

- [60] I. Bautista, C. Pajares, and J. Dias de Deus, Nucl. Phys. **A882**, 44 (2012).
- [61] I. Bautista, J. Dias de Deus, G. Milhano, and C. Pajares, Phys. Lett. **B715**, 230 (2012).
- [62] I. Bautista, C. Pajares, G. Milhano, and J. Dias de Deus, Phys. Rev. **C86**, 034909 (2012).
- [63] C. Merino, C. Pajares, and Yu.M. Shabelski, arXiv:1207.6900[hep-ph].
- [64] J. Dias de Deus and C. Pajares, Phys. Lett. **B695**, 211 (2012) and arXiv:1011.1099[hep-ph].
- [65] T. Anticic *et al.*, NA49 Collaboration, arXiv:1004.1889[hep-ex].
- [66] T. Alber *et al.*, NA35 Collaboration, Eur. Phys. J. **C2**, 643 (2008) and arXiv:9711001[hep-ex].
- [67] G. Bearden *et al.*, NA44 Collaboration, Phys. Rev. **C57**, 837 (19988) and arXiv:9711004[nucl-ex].
- [68] T. Anticic *et al.*, NA49 Collaboration, Phys. Rev. **C80**, 034906 (2009) and arXiv:0906.0469[nucl-ex].
- [69] F. Antinori *et al.*, NA57 Collaboration, J. Phys. **G32**, 427 (2006) and arXiv:0601021[nucl-ex].
- [70] M.M. Aggarwal *et al.*, STAR Collaboration, Phys. Rev. **C83**, 024901 (2011) and arXiv:1010.0142[nucl-ex].
- [71] G. Agakishiev *et al.*, STAR Collaboration, Phys. Rev. Lett. **108**, 072301 (2012) and arXiv:1107.2955[nucl-ex].